Ferroelastic phase transitions and anelastic dissipation in the $LaAlO_3$-$PrAlO_3$ solid solution series

R. I. Thomson,[1,2] J. M. Rawson,[2] C. J. Howard,[3] S. Turczynski,[4] D. A. Pawlak,[4] T. Lukasiewicz,[4] and M. A. Carpenter[1]
[1]*Department of Earth Sciences, University of Cambridge, Downing Street, Cambridge CB2 3EQ, United Kingdom*
[2]*Department of Chemistry, University of Cambridge, Lensfield Road, CB2 1EW Cambridge, United Kingdom*
[3]*School of Engineering, University of Newcastle, New South Wales 2308, Australia*
[4]*Institute of Electronic Materials Technology, ul. Wolczynska 133, PL-01 919 Warsaw, Poland*
(Received 3 August 2010; published 15 December 2010)

Resonant ultrasound spectroscopy has been used on single-crystal samples to observe pseudoproper ferroelastic softening across the $(La,Pr)AlO_3$ solid solution. It is suggested that softening is due to the presence of an intrinsic zone-center instability in addition to the small Jahn-Teller stabilization expected for Pr^{3+}. Softening increases as smaller Pr^{3+} ions are substituted for larger La^{3+} which is attributed to a simple size effect as well as the possibility of bilinear coupling of the intrinsic instability with the weak Jahn-Teller effect. Superattenuation is observed above 600 K for all samples, which is consistent with twin wall related dissipation behavior seen in other perovskites with octahedral tilting. Superattenuation is also observed in the low-temperature monoclinic phase, implying a high mobility also for the monoclinic twin walls.

DOI: 10.1103/PhysRevB.82.214111 PACS number(s): 62.20.D−, 74.62.−c, 63.70.+h

I. INTRODUCTION

Perovskites (ABO_3) are well known to undergo phase transitions as a result of changes in temperature and composition. Composition-dependent phase transitions occur as a result of substitution of a different metal cation onto either the *A* or *B* sites. For example, substitution of Ti for Zr in $Sr(Zr,Ti)O_3$ causes the temperatures of the octahedral tilting transitions to be suppressed, favoring progressively higher symmetry orthorhombic, tetragonal, and cubic crystals to become stable at room temperature.[1] Another important mechanism for driving transitions in perovskites is via octahedral distortions due to the Jahn-Teller effect but many solid solutions display both tilting and Jahn-Teller instabilities.[2] Despite the small energy associated with Jahn-Teller distortions of lanthanides, the $LaAlO_3$-$PrAlO_3$ solid solution is often cited as an example of a Jahn-Teller-driven instability.[3] In such systems, the properties which are most sensitive to the mechanism and thermodynamic character of the transitions are the elastic constants. In an octahedral tilting transition which is second order there is a stepwise change in the elastic constants due to the coupling of the symmetry-breaking strain with the square of the order parameter *q* (an improper ferroelastic transition). On the other hand a Jahn-Teller distortion can cause the transition to be pseudoproper ferroelastic (as defined by Wadhawan 1982) (Ref. 4) in character with a minimum in the elastic constants and nonlinear softening on either side of the transition (e.g., Carpenter and Salje 1998).[5] In this case the symmetry-breaking strain couples bilinearly with the order parameter. In principle, a soft acoustic mode might cause a proper ferroelastic transition, where the symmetry-breaking strain is the order parameter for the transition. The elastic constants go to a minimum with linear softening on either side of the transition point. In each case observed variations of the elastic constants could be indicative of the driving mechanism.

In the general context of the elastic behavior of perovskites, one system that is of particular interest is $PrAlO_3$ because it undergoes transitions due to coupling of tilting and electronic effects. Our understanding of the sequence of transitions in $PrAlO_3$ has been steadily refined with increasing data quality. The most recent neutron powder-diffraction studies have produced: $Pm\bar{3}m$-$R\bar{3}c$ (1864 K, second order), $R\bar{3}c$-*Imma* (210–220 K, first order), and *Imma*-$C2/m$ (151 K, second order).[3,6] The cubic-rhombohedral transition is due to octahedral tilting but the orthorhombic phase is stabilized in part by Jahn-Teller distortions and the orthorhombic to monoclinic phase transition is believed to be driven entirely by Jahn-Teller distortions around the Pr^{3+} center.[7] This sequence fits into the broader range of possibilities as may be deduced for all possible combinations of R_4^+ (tilting) and Γ_3^+ (Jahn-Teller) instabilities. A possible hierarchy of tilting followed by Jahn-Teller transitions is shown in Fig. 1 from Carpenter *et al.*[8]

The primary objective of the present study was to determine the elastic and anelastic behavior of perovskites in the solid solution between $LaAlO_3$, which undergoes tilting only, and $PrAlO_3$ which undergoes both tilting and Jahn-Teller transitions. This system was chosen first because of its known subsolidus phase relations (Fig. 2) and because an unexpected incipient elastic instability has been previously detected in $LaAlO_3$.[11] The phase diagram shows a high-temperature tilting transition ($Pm\bar{3}m$-$R\bar{3}c$) extending across the solid solution, together with a low-temperature stability field for the *Imma* structure, which pinches out at $\sim Pr_{0.3}La_{0.7}AlO_3$, and a $C2/m$ stability field which approaches 0 K at $\sim Pr_{0.1}La_{0.9}AlO_3$. It would be surprising to find a strong Jahn-Teller contribution from Pr^{3+} extending so far across the solid solution and the suspicion must be that other factors could be responsible for both the elastic softening observed in $LaAlO_3$ and for the appearance of a monoclinic phase at La-rich compositions. A recent study of $PrAlO_3$ has revealed substantial elastic softening over a wide temperature interval between ~150 K and at least ~600 K by resonant ultrasound spectroscopy (RUS) (Ref. 8). In the present study the same pattern of softening has been followed in single crystals across the entire solid solution. At the same time, anelastic dissipation at high temperatures fol-

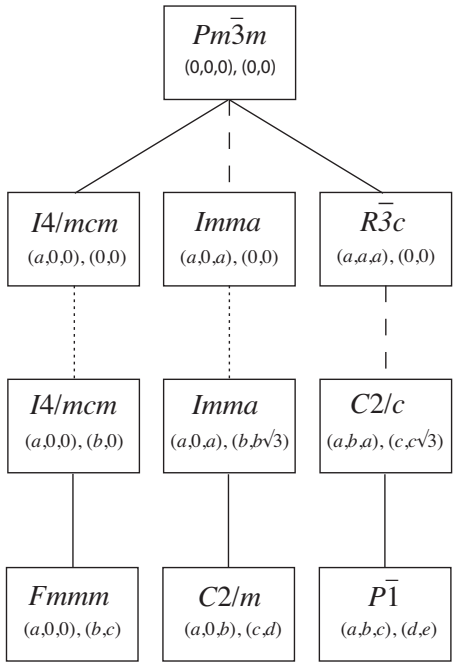

FIG. 1. Hierarchy of possible phase transitions in $LaAlO_3$-$PrAlO_3$ due to octahedral tilting (three-component order parameter transforming as irrep R_4^+) and cooperative Jahn-Teller distortions (two-component order parameter transforming as irrep Γ_3^+), from Carpenter *et al.* (Ref. 8). Different nonzero R_4^+ components first give the tilted structures and then Γ_3^+ components are added. Solid lines represent transitions which are allowed by symmetry to be second order in character, broken lines are required to be first order and dotted lines represent isosymmetric transitions.

lows the pattern established in $LaAlO_3$[12] and $PrAlO_3$,[8] which is believed to be due to mobility under stress of twin walls arising at the tilting transition. Strong attenuation of acoustic resonances (superattenuation) in the monoclinic structure is also reported.

$LaAlO_3$ is widely used as a substrate for thin films with diverse properties[13–16] and in sandwich materials interlayered with $SrTiO_3$ to produce unusual electrical properties.[17–19] Since strain is known to be important in these types of materials, additional elastic relaxations achieved by adjusting the chemistry of the $LaAlO_3$ layers might, in principle, provide an additional variable with which to control their properties. Within this context resonant ultrasound spectroscopy provides an excellent characterization tool with which to probe the origin of their response.

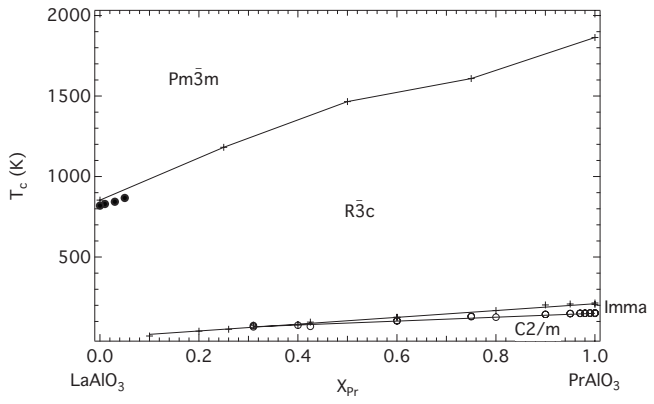

FIG. 2. $PrAlO_3$-$LaAlO_3$ phase diagram based on data from the literature (Refs. 3, 9, and 10) with high-temperature phase transitions for compositions Pr_0, Pr_1, Pr_3, and Pr_5 from the present study shown as filled circles.

Elastic softening mechanism

In order to understand the patterns of pseudoproper elastic softening observed in $(La,Pr)AlO_3$ samples, it is necessary to briefly review the possible influence of the Jahn-Teller contributions. Carpenter *et al.*[3] produced a Landau expansion for coupled R_4^+ tilting and Γ_3^+ Jahn-Teller ordering. For present purposes two equations are worth reproducing. First, ignoring saturation terms, a second-order Jahn-Teller transition with critical temperature $T_{c,JT}$ would actually occur at a higher temperature $T^*_{c,JT}$ due to bilinear coupling of the order parameter with the symmetry-breaking strain. If the coupling coefficient is λ_t, $T_{c,JT}$, and $T^*_{c,JT}$ are related by

$$T^*_{c,JT} = T_{c,JT} + \frac{\lambda_t^2}{a_{JT}\frac{1}{2}(C^0_{11} - C^0_{12})}, \tag{1}$$

where a_{JT} is the Landau coefficient for the second order term and C^0_{11}, C^0_{12} are elastic constants of the reference cubic phase. Second, as the temperature approaches $T^*_{c,JT}$ from above acoustic softening would occur according to the following expression:

$$(C_{11} - C_{12}) = (C^0_{11} - C^0_{12})\left(\frac{T - T^*_c}{T - T_c}\right). \tag{2}$$

Below the transition temperature $(C_{11}-C_{12})$ would be expected to recover nonlinearly, as expected for a pseudoproper ferroelastic transition.[5,20]

Pseudoproper ferroelastic softening behavior would be somewhat different in a rhombohedral crystal. The elastic stability limit is given by the eigenvalues of the elastic constant matrix.[21] For a crystal belonging to the class $\bar{3}m$ with respect to a trigonal reference system (indicated by the subscript T) this gives

$$(C_{11T} - C_{12T})C_{44T} - 2C^2_{14T} > 0. \tag{3}$$

With respect to a cubic reference system the stability limit becomes

$$(C_{11} - C_{12})C_{44} > 0. \tag{4}$$

Therefore the combination $(C_{11}-C_{12})C_{44}$ would be expected to tend to zero as T approaches T^*_c, in the same manner as described by Eq. (2). This behavior would lead to the formation of a $C2/c$ monoclinic structure however, as opposed to the $C2/m$ structure which is observed. The $C2/m$ structure can only be reached by an intermediate stage in which a first-order transition to the *Imma* structure occurs. This is stabilized by a component of the Γ_3^+ order parameter, q_{tx}, where

$$q_{tx} = \frac{1}{2}(q_{tz} + \sqrt{3}q_{oz}). \quad (5)$$

The condition for stability of the *Imma* structure with respect to the expected $C2/m$ structure is $C_{55} > 0$ and this becomes $(C_{11} - C_{12}) > 0$ for cubic reference axis. Elastic softening as the *Imma*-$C2/m$ transition is approached should have the same form as Eq. (2) and C_{44} should not exhibit the same softening behavior. The *Imma*-$C2/m$ transition is driven by the second Γ_3^+ order parameter component, q_{ox}, where

$$q_{ox} = \frac{1}{2}(\sqrt{3}q_{tz} - q_{oz}). \quad (6)$$

The other end member of the solid solution series investigated in the present study, $LaAlO_3$, is not expected to show elastic softening ahead of the octahedral tilting transition point, as it is improper, and La is not expected to induce Jahn-Teller distortions due to its different electronic configuration, i.e., a spherically symmetric electron distribution (La^{3+} $4f^0$).

II. EXPERIMENTAL DETAILS

A. Sample preparation

Crystal growth. $Pr_xLa_{1-x}AlO_3$ crystals, where $x = 1, 0.75, 0.55, 0.4, 0.05, 0.03, 0.01, 0$, were grown using the Czochralski method.[22] These are labeled Pr_{100}, Pr_{75}, Pr_{55}, Pr_{40}, Pr_5, Pr_3, Pr_1, and Pr_0 throughout the rest of this paper. As described already for growth of the Pr_{100} crystal,[23] the raw materials used were high purity Pr_6O_{11}, Al_2O_3, and La_2O_3 oxides (99.995%). All components were mixed in stoichiometric ratios. A conventional Czochralski apparatus, Oxypuller 0503 (Cyberstar), and rf heating were used. The crystals were grown in a nitrogen atmosphere from an iridium crucible, 50 mm in diameter and height. The pulling and rotation rates were 1–1.7 mm/h and 6–8 rpm, respectively. Crystals which were approximately 20 mm in diameter and 50 mm long were seed grown with iridium wires.

Single crystals were cut as approximately $5 \times 4 \times 3$ mm^3 parallelepipeds. In terms of a cubic reference system the 5×4 mm^2 side of each parallelepiped was parallel to (001) and the 4×3 mm^2 side was parallel to (110). Three surfaces were polished, two parallel to (001) and one parallel to (110). Investigation under an optical microscope revealed that the crystals were finely twinned. Table I lists the dimensions, masses, and colors of the various samples used. Note that the Pr_3 crystal was smaller than the others. After heating in air during RUS measurements all samples underwent a color change, emerging darker than they had been at the start. This effect was most pronounced in samples with high Pr contents.

B. RUS apparatus

The RUS setup for high-temperature measurements consists of two alumina rods mounted horizontally in a Netzsch 1600 °C furnace.[24] The sample is held lightly across a pair of corners between the ends of the rods within the furnace. Piezoelectric transducers are attached to the other ends of the rods outside the furnace. One transducer is the driving resonator and the other is the detector and data are collected using Stanford electronics.[25] In the low-temperature head the sample is placed across a pair of faces between the two transducers in a mount which is lowered vertically into a helium flow cryostat, as described by McKnight *et al.*[26]

TABLE I. Dimensions, mass, and color of single crystals used for RUS.

Composition	Dimensions (mm^3)	Mass (g)	Color before heating
Pr_{100}	$4.963 \times 3.937 \times 3.025$	0.3922	Dark green
Pr_{75}	$4.776 \times 3.816 \times 3.008$	0.3583	Bright green
Pr_{55}	$4.833 \times 3.824 \times 3.002$	0.3599	Bright green
Pr_{40}	$4.893 \times 3.889 \times 3.034$	0.3749	Orange/brown
Pr_5	$5.017 \times 4.006 \times 3.217$	0.4189	Pale brown
Pr_3	$4.107 \times 3.474 \times 3.166$	0.2897	Pale orange/brown
Pr_1	$5.025 \times 4.029 \times 3.184$	0.4156	Colorless
Pr_0	$5.023 \times 4.142 \times 3.244$	0.4372	Pale pink

C. Data collection and analysis

For this study separate RUS measurements were made at room temperature, low temperatures and high temperatures as follows.

Room temperature. Spectra containing 20 000 data points were collected from all samples in the frequency range 100–1200 kHz. The measurements were repeated with each crystal held in five different orientations to ensure that all resonances were excited and observed.

Low temperature. Data were collected at low temperature with the sample chamber filled with a few millibar of helium to allow heat exchange between the sample and the cryostat. Due to occasional leaks, the pressure in the sample chamber was higher for some runs but this is not thought to have affected the results. For all the samples the system was cooled from 280 to 10 K in 30 K steps with a 1200 s settle time at each temperature to allow for thermal equilibration. For Pr_0, Pr_1, Pr_3, and Pr_5 spectra containing 50 000 data points were collected in the frequency range 50–1200 kHz, and for all other compositions in the range 100–1200 kHz.

The samples were then heated and data collected at different temperature intervals for different compositions as follows: Pr_0, Pr_1, Pr_3, Pr_5, Pr_{55}, and Pr_{75} 10–295 K in 5 K steps; Pr_{40} 10–100 K in 2 K steps, 100–290 K in 5 K steps; Pr_{100} 10–110 K in 5 K steps, 110–130 K in 2 K steps, 130–140 K in 5 K steps, 140–160 K in 2 K steps, 160–195 K in 5 K steps, 195–215 K in 2 K steps, and 215–295 K in 5 K steps.

Additional spectra were taken to look more closely at the data around the phase transitions for the Pr_{55} and Pr_{75} compositions as follows: Pr_{75} 280–130 K in 30 K steps then heated 130–163 K in 2 K steps, 164–284 K in 30 K steps, and 284–295 K in one 11 K step; Pr_{55} 290–80 K in 30 K steps then heated; 80–134 K in 2 K steps and 134–284 K in 30 K steps. In each case the frequency range was 100–1200 kHz and 50 000 data points were collected.

High temperature. The samples were loaded onto the high-temperature head and data were collected during heating and cooling sequences with an equilibration time of 15 min at each temperature. Pr_0 was cooled from 826 to 812 K in 2 K steps, 812 to 292 K in 20 K steps. Pr_1 was cooled from 830 to 790 K in 2 K steps, 790 to 290 K in 20 K steps. Pr_3 was cooled from 890 to 830 K in 2 K steps, 830 to 290 K in 20 K steps. Pr_5 was heated from 290 to 820 K in 10 K steps, 820 to 853 K in 1 K steps, 853 to 1043 K in 10 K steps, then cooled 1043 to 293 K in 50 K steps. A second run was done involving heating from 865 to 886 K in 1 K steps to locate the transition. Pr_{40} and Pr_{55} were cooled from 830 to 290 K in 10 K steps. Pr_{75} was cooled from 830 to 290 K in 20 K steps. Pr_{100} was heated from 300 to 750 K in 10 K steps and then cooled from 700 to 300 K in 10 K steps. All data were collected in the frequency range 100–1200 kHz except Pr_5 and Pr_{100} which were analyzed across the ranges 200–1400 kHz and 200–1200 kHz, respectively. For samples Pr_1, Pr_5, Pr_{55}, Pr_{75} and Pr_{100}, 20 000 data points were collected and for all other samples 12 000 data points were collected per spectrum. Temperature was calibrated against the α-β transition of quartz (846 K).[27]

All spectra were transferred to the software package IGOR PRO (WaveMetrics) for analysis. Peak positions and widths at half height were determined for a selection of peaks by fitting with an asymmetric Lorentzian function. The quality factor, Q, was calculated using the relationship $Q=f/\Delta f$, where f is the peak frequency and Δf is the width of the peak at half its maximum height. The inverse of the quality factor, Q^{-1}, is a measure of acoustic dissipation in the sample.

III. RESULTS

A. Raw data

To illustrate general features of the raw data, low-temperature spectra from Pr_{100}, Pr_{75}, and Pr_{55} are shown as stacks in Fig. 3 and high-temperature spectra from Pr_1 and Pr_{55} are displayed in Fig. 4. These stacks show how peak frequencies change as a function of temperature and reveal sudden changes in trend due to phase transitions. Peaks in the spectra that are affected by temperature represent the vibrational frequencies of the normal modes of the sample and the square of the frequency of each mode is directly proportional to the elastic constants associated with that mode.[28] Temperature-independent peaks at lower frequency (for example, at 120 and 190 kHz) are noise from the RUS head.

With respect to a cubic reference system, the frequencies of individual peaks are largely determined by combinations of the elastic constants $\frac{1}{2}(C_{11}-C_{12})$ and C_{44}, with only a small contribution from the bulk modulus, $K=\frac{1}{3}(C_{11}+2C_{12})$. Average values of cubic elastic constants, $\frac{1}{2}(C_{11}-C_{12})$ and C_{44} have been determined previously for $LaAlO_3$ by fitting between 20 and 30 peaks using the software described by Migliori and Sarrao.[28] Good fits were obtained, on the basis that twin orientations must have been significantly random that the average symmetry was cubic.[12] Attempts to fit room-temperature data for $PrAlO_3$ in the present study (and see Ref. 8) were not successful however due to some preferred orientation of the twins such that the effective macroscopic symmetry of the crystal, i.e., the average over all twin domains, is not cubic. In $LaAlO_3$ values of the elastic constants are $\frac{1}{2}(C_{11}-C_{12})=61$ GPa and $C_{44}=145$ GPa.[12] It is anticipated that C_{44} will also be greater than $\frac{1}{2}(C_{11}-C_{12})$ across the $(La,Pr)AlO_3$ solid solution and, as a consequence, the resonance peaks with lowest frequency will depend predominantly on $\frac{1}{2}(C_{11}-C_{12})$. The other lowest frequency peaks will depend predominantly on $\frac{1}{2}(C_{11}-C_{12})$ or C_{44} while higher frequency peaks will depend predominantly on a mixture of these two shear elastic constants.

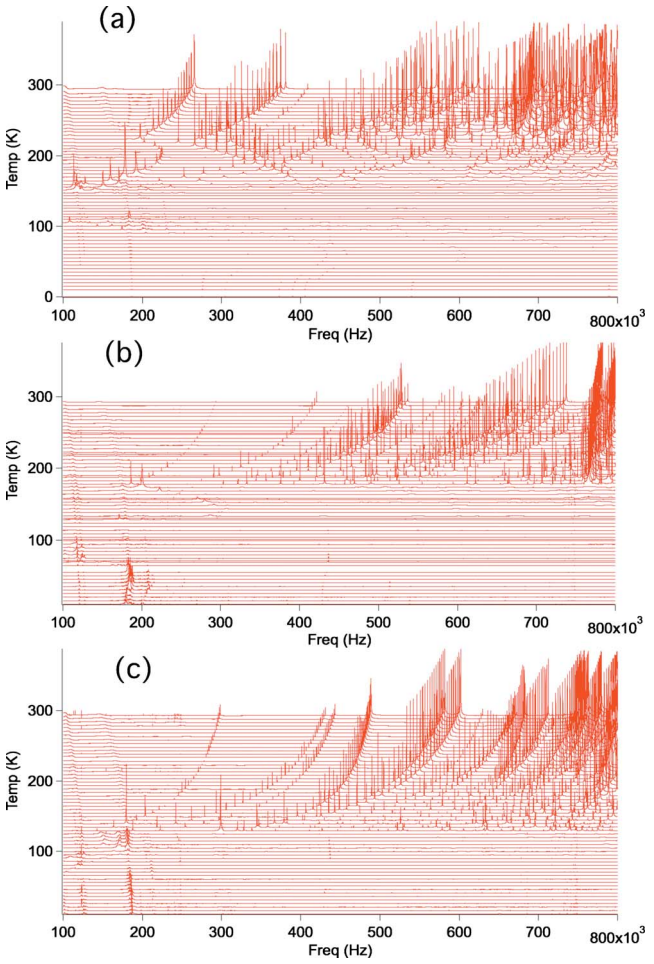

FIG. 3. (Color online) Low-temperature RUS stacks for (a) Pr_{100}, (b) Pr_{75}, and (c) Pr_{55}. In (a) differences in the behavior of the elastic constants are illustrated by the first two peaks in the spectra. Weak peaks present at low frequency and low temperature are due to noise from the RUS instrumentation.

Figure 3(a) shows the low-temperature stack for $PrAlO_3$. Two different patterns of behavior can be seen in the peaks, represented very clearly by the two peaks with the lowest frequencies. On reducing temperature both peaks show a significant elastic softening until 223 K ($R\bar{3}c$-*Imma* transition). The lowest frequency peak, attributed to $\frac{1}{2}(C_{11}-C_{12})$ recovers slightly before further softening to approximately 157 K (*Imma*-$C2/m$ transition). The second peak, believed to represent C_{44}, does not show any further softening and contin-

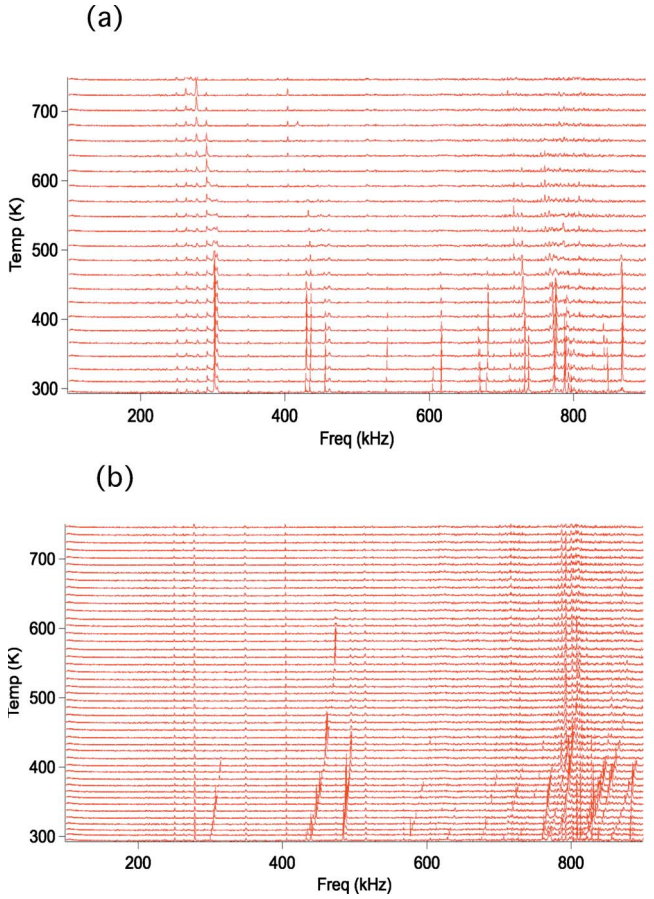

FIG. 4. (Color online) Portions of (a) Pr_1 and (b) Pr_{55} high-temperature stacks. Note that resonance peaks disappear above ~600 K as in $LaAlO_3$ (Ref. 12). Weak peaks that do not change frequency with increasing temperature are from the alumina rods and not from the sample.

ues to recover until the peaks disappear at the orthorhombic-monoclinic phase transition. As is seen in Fig. 3, evolution of peaks in the stability field of the *Imma* structure is harder to follow in spectra from Pr_{75} and Pr_{55}.

Below the $R\bar{3}c$-*Imma* phase transition, shown by the sudden change in peak frequency at 223 K, 178 K, and 129 K in Pr_{100}, Pr_{75} and Pr_{55}, respectively, there is a change in peak intensity. For Pr_{100}, peaks are still visible well into the *Imma* stability field and some peaks are visible down to the *Imma*-$C2/m$ transition. After this the peaks disappear entirely though there is a reappearance of some low frequency peaks at approximately 114 K. In Pr_{75} and Pr_{55} the only peak present in spectra collected in the *Imma* stability field is that with the very lowest frequency.

At high temperatures, all resonance peaks disappear from spectra collected at temperatures above ~600 K for all the crystals examined. This is the same as observed for $LaAlO_3$[12] and is shown for Pr_1 and Pr_{55} in Fig. 4.

B. Changes in f^2 and Q^{-1}

Figure 5 shows the temperature dependence of the square of the frequency for selected low-frequency peaks for all the

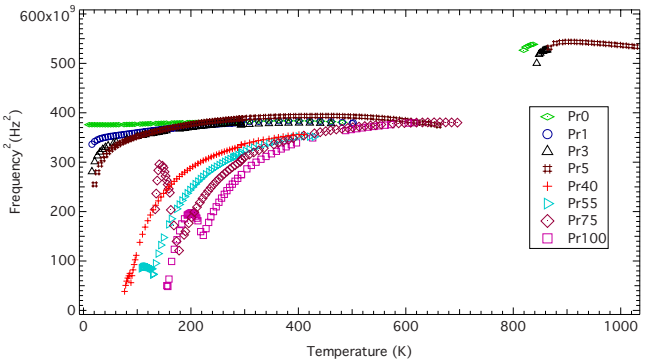

FIG. 5. (Color online) Changes in the square of the peak frequency (which is proportional to the elastic constants) with temperature for all compositions across the solid solution. Values of frequency squared have been scaled to the same value at 600 K for easier comparison between compositions. Peaks used are those that are at the lowest frequency, except in Pr_0 where a peak at a higher frequency was used as it could be followed to a lower temperature and so could better represent the elastic behavior. Small offsets at 300 K are due to the change between high- and low-temperature RUS instruments.

samples. These values of f^2 are believed to display, predominantly, the variation in $\frac{1}{2}(C_{11}-C_{12})$. For comparative purposes and in the absence of absolute values of the elastic constants, they have been scaled to a fixed value at 600 K. Samples which did not display peaks to this temperature were scaled via extrapolation to 600 K. Minima in f^2 for the compositions Pr_{100} to Pr_{40} represent the $R\bar{3}c$-*Imma* phase transition. Following the first phase transition, Pr_{100}, Pr_{75}, Pr_{55}, and Pr_{40} show some elastic stiffening to a distinct maxi-

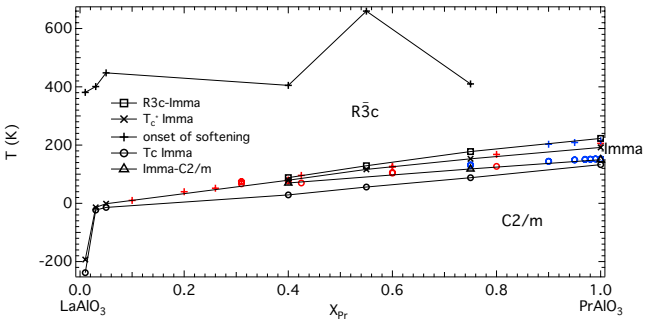

FIG. 6. (Color online) Low-temperature part of the $LaAlO_3$-$PrAlO_3$ phase diagram with transition temperatures from the present study shown as open squares and triangles joined by lines. The values for the transition temperatures came from minima in the square of the peak frequencies for the $R\bar{3}c$-*Imma* transition and the point where the f^2 values in Fig. 5 extrapolated to zero for the *Imma*-$C2/m$ transition. Values of T_c^* are shown as crosses (x) joined by a line and T_c by open circles joined by lines; these were obtained by fitting Eq. (2) to data in the $R\bar{3}c$ stability field. Crosses (+) represent the temperature at which a softening trend with falling temperature became established in the $R\bar{3}c$ stability field. Red and blue crosses and open circles are data from the literature (Refs. 3, 9, and 10).

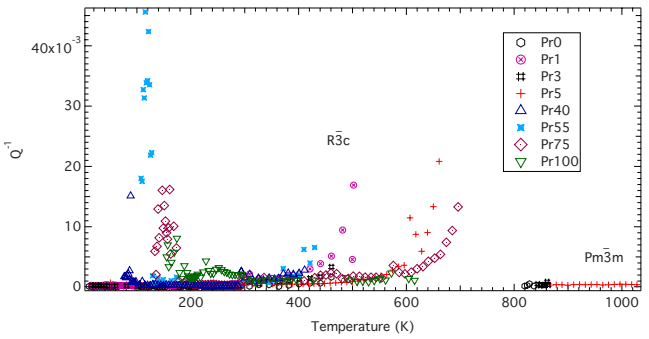

FIG. 7. (Color online) Changes in the inverse quality factor as a function of temperature. Increase in Q^{-1} indicates increase in acoustic dissipation in the sample. Discrepancies at 300 K are due to a change in instrumentation between high- and low-temperature heads.

mum. All four compositions show softening until the peaks disappear in the vicinity of the *Imma*-$C2/m$ transition. It can be seen from the data that the temperature of the transitions decreases with decreasing praseodymium content. Temperatures for the $R\bar{3}c$-*Imma* phase transition were taken simply as the temperature which f^2 was a minimum. Temperatures for the *Imma*-$C2/m$ transition were estimated by extrapolating f^2 to zero for the lowest temperature data points from spectra in which resonance peaks could still be identified. These have been added to the data from the literature in Fig. 6.

For the compositions Pr_0, Pr_1, Pr_3, and Pr_5 the $R\bar{3}c$-*Imma* phase transition does not take place. Significant elastic softening with falling temperature still occurs, however. This reduces with reducing Pr content but $LaAlO_3$ still shows slight softening with falling temperature between 400 and 50 K,[11] which can just be seen in Fig. 5. The softening in Pr_1, Pr_3, and Pr_5 resembles softening at higher temperatures in other crystals. At these compositions high-temperature data for f^2 show that the $Pm\bar{3}m$ structure is elastically stiffer than the $R\bar{3}c$ structure (Fig. 5).

Figure 7 shows the variations in Q^{-1} for all studied compositions determined from the same peaks as used to obtain the f^2 data shown in Fig. 5. Q^{-1} is small ~0.0001 (low dissipation) within the $R\bar{3}c$ stability field for La-rich compositions down to 10 K. It is similarly low in Pr-rich compositions above the $R\bar{3}c$-*Imma* transition. Some increase is observed in the *Imma* stability field as the *Imma*-$C2/m$ phase transition is approached. No variation in Q^{-1} is seen for the *Imma*-$R\bar{3}c$ phase transition except in Pr_{100} (~225 K) where there is a slight increase in acoustic dissipation. The steep rise in Q^{-1} as the *Imma*-$C2/m$ transition is approached is followed by complete disappearance of resonance peaks from spectra within the stability of the $C2/m$ structure. Only in the vicinity of 100 K for Pr_{100} do a few resonance peaks reappear [Fig. 3(a)].

At higher temperatures there is an increase in Q^{-1} for all samples corresponding to the strong attenuation due to twin wall mobility described in detail for $LaAlO_3$ by Carpenter *et al.*[12] Above ~550–600 K, resonance peaks disappeared from spectra obtained from all the samples, only to reappear with low-Q^{-1} values in the stability field of the $Pm\bar{3}m$ structure for Pr_0, Pr_1, Pr_3, and Pr_5 (Figs. 4 and 5). The $Pm\bar{3}m$-$R\bar{3}c$ transition temperature in these La-rich compositions has been taken as the temperature between the last spectrum at which peaks were absent and the first at which they were present. These transition temperatures are listed in Table II and are shown in Fig. 2.

C. Elastic softening parameters

Following Eqs. (2) and (4), fits were made to the frequency-squared data over wide temperature intervals in the stability field of the $R\bar{3}c$ structure using the expression:

$$f^2 = f_0^2\left(\frac{T - T_c^*}{T - T_c}\right), \tag{7}$$

where T_c is the transition temperature in the absence of strain order-parameter coupling and T_c^* is the renormalized transition temperature due to this coupling. T_c^* is never reached because the first-order phase transition to the *Imma* phase occurs first. Values of T_c^* are displayed on the low-temperature phase diagram in Fig. 6. Values of T_c and T_c^*

TABLE II. Values, where available, for transition temperatures, T_c and T_c^* for all transitions and for the onset of softening in each sample.

	$Pm\bar{3}m$-$R\bar{3}c$	$R\bar{3}c$-*Imma*			(*Imma*,$R\bar{3}c$)-$C2/m$			
Composition	T_{trans} (K)	T_{trans} (K)	T_c^* (K)	T_c (K)	T_{trans} (K)	T_c^* (K)	T_c (K)	$T_{softening}$ (K)
Pr_{100}		223	192	133	150	151	113	>620
Pr_{75}		178	153	88	118			410
Pr_{55}		129	117	56				660
Pr_{40}		88	79	29	70			495
Pr_5	867					−1	−14	448
Pr_3	843					−14	−24	401
Pr_1	830					−193	−238	381
Pr_0	819							250

obtained from the fitting are given in Table II. The high-temperature onset of softening has been determined by differentiating f^2 with respect to temperature and the resulting values added to Fig. 6 and Table II.

IV. DISCUSSION

A. Elastic behavior of $PrAlO_3$

In the $R\bar{3}c$ stability field of $PrAlO_3$ all the resonance peaks shift to lower frequency with falling temperature, which implies that both $\frac{1}{2}(C_{11}-C_{12})$ and C_{44} are softening. This is consistent with the stability limit of $\frac{1}{2}(C_{11}-C_{12})C_{44} \rightarrow 0$ as T approaches T_c^*, for a $C2/c$ structure. This transition point is not reached, however, which is consistent with the view that pseudoproper ferroelastic behavior in the system is driven in part at least by linear coupling of the strain and the Γ_3^+ order parameter and that this stabilizes the *Imma* structure first, followed by the $C2/m$ structure. The observation of two different modes of softening and stiffening in the *Imma* field of Pr_{100} is also consistent with this model, as set out in Sec. I, since $\frac{1}{2}(C_{11}-C_{12})$ is expected to soften in the *Imma* stability field while C_{44} is not. The value of $T_c^*-T_c=59\pm2$ K from fitting in the $R\bar{3}c$ field provides a measure of the strength of the coupling between the driving order parameter and the symmetry-breaking strain [Eq. (1)]. Equivalent fitting to data between 189 and 157 K in the stability field of the *Imma* structure gives $T_c^*-T_c=38$ K (T_c^* fixed at 151 K, $T_c=113$ K) but at least some of the curvature in the primary data may be due to the $R\bar{3}c$-*Imma* transition.

As the $R\bar{3}c$-*Imma* transition is first order it is expected that there will be a discontinuity in the elastic properties at the transition temperature. This is not observed in $PrAlO_3$ and there is significant non linear elastic softening on both sides of the transition, implying that the transition does not involve a discontinuous switch from one phase to the other but that there are some premonitory effects in both phases. The same pattern of behavior has been observed at the $R\bar{3}c$-*Imma* transition in $BaCeO_3$[29] and at the $I4/mcm$-*Imma* transition in $SrZrO_3$.[27] McKnight *et al.*[27] suggested that there is dynamic clustering of each tilt system within local regions of the crystal ahead of the actual transition point.

B. Effect of solid solution on phase transitions and elastic behavior

The uniform trends with composition for transition points and other temperatures shown in Figs. 2 and 6 can be explained most simply in terms of cation size effects. For octahedral tilting, for example, the tilt instability can be understood as arising simply from average ratios for the cations occupying A and B sites of the perovskite structure in the usual way. Tabulated radii of the ions are: $La^{3+}=103.2$ pm, $Pr^{3+}=99.0$ pm.[30] Substitution of La^{3+} into $PrAlO_3$ or Pr^{3+} into $LaAlO_3$ therefore creates local strain fields. As soon as there are enough impurity sites in the crystal such that the strain fields overlap, the transition temperature will be affected and it has been shown that only 1% doping of La^{3+} into $PrAlO_3$ is required for this to occur.[31] The 4% difference in radius is then significant enough to change the tilting transition temperature by ~1000 K and the lower temperature transitions by ~200 K.

Similarly, the patterns of elastic softening appear to vary uniformly across the solid solution. Frequencies of resonance peaks attributed to $\frac{1}{2}(C_{11}-C_{12})$ in Pr_{40}, Pr_{55}, and Pr_{75} display stiffening and softening which is essentially the same as in Pr_{100}, though displaced to lower temperatures (Fig. 5). The fit parameters T_c^* and T_c from softening in the $R\bar{3}c$ stability field vary almost linearly with composition across the solid solution, and data for T_c^* from Pr_3 and Pr_5 lie directly on the extrapolation of data for Pr_{100}-Pr_{40} and on the extrapolation of the rhombohedral-monoclinic transition in the La-rich half of the solid solution (Fig. 6). Only the value of T_c^* for Pr_1 falls off this latter trend. The onset temperature for elastic softening in the $R\bar{3}c$ stability field shows more scatter (Fig. 6) but no real evidence for any discontinuity in behavior. A remarkable feature of the elastic softening, however, is the fact that Pr^{3+} can be Jahn-Teller active while La^{3+} cannot, and it seems unlikely that the softening is attributable solely to electronic orbital effects. Furthermore, the energy of the Jahn-Teller effect for Pr^{3+} is likely to be small, according to the following argument.

The valence orbitals in Pr^{3+} are f orbitals which are extremely radially contracted. In the presence of a cubic ligand field these are split into three sets of degenerate orbitals of a_{2u}, t_{2u}, and t_{1u} symmetry as displayed in Fig. 2 of Atanasov *et al.*[32] Under octahedral symmetry Δ_1 is approximately 462 cm^{-1} and Δ_2 is 1172 cm^{-1}.[32] Under eightfold coordination the crystal-field splitting parameter is approximately 450 cm^{-1}.[33] Increasing the coordination of the Jahn-Teller ion takes the overall symmetry closer to spherical and should therefore decrease the amount of crystal field splitting. In this perovskite system the Pr^{3+} is 12 coordinate and therefore the crystal-field splitting parameter should be less than 450 cm^{-1}. If the crystal-field splitting parameter is of the order of 500 cm^{-1} then the Jahn-Teller splitting, δ, would likely offer an upper limit of 50 cm^{-1} and the stabilization from occupation of these lower-lying orbitals will only be approximately 5 cm^{-1} for 10% doping, which corresponds to a transition temperature of around 8 K. The transitions in this solid solution are all well above this temperature and so it is very unlikely that a Jahn-Teller distortion alone could be responsible for them and an additional driving mechanism must exist.

All the softening observed across the solid solution is nonlinear with temperature, so any additional driving order parameter must also give pseudoproper ferroelastic character. The most obvious mechanism would involve a soft optic mode which is intrinsic to the structure and couples bilinearly with a soft acoustic mode. The order parameter would have Γ_3^+ symmetry with respect to space group $R\bar{3}c$ and would lead to a first-order (due to third order invariants) transition $R\bar{3}c$-$C2/c$. With respect to space group $Pm\bar{3}m$ the order parameter could have Γ_3^+ or Γ_5^+ symmetry since both these irreducible representations (irreps) appear in space groups $C2/m$ and $C2/c$ (Table III); Γ_3^+ could be the primary irrep and Γ_5^+ a secondary irrep, or vice versa. In effect the solid solution would then behave slightly differently at Pr-

TABLE III. All irreps and their nonzero components for space groups $C2/c$ and $C2/m$ with respect to parent space group $Pm\bar{3}m$. Note that in each case Γ_3^+ could be the primary order parameter and Γ_5^+ a secondary order parameter or vice versa.

Space group $C2/c$ with lattice vectors $(2,-1,-1)(0,1,-1)(0,1,1)$, origin $(\frac{1}{2},\frac{1}{2},0)$		
Irrep	Components	Subgroup
Γ_1^+	(a)	$Pm\bar{3}m$
Γ_3^+	$(a,a\sqrt{3})$	$P4/mmm$
Γ_4^+	$(0,a,-a)$	$C2/m$
Γ_5^+	(a,b,a)	$C2/m$
R_2^+	(a)	$Fm\bar{3}c$
R_3^+	$(a,-a/\sqrt{3})$	$I4/mcm$
R_4^+	(a,b,a)	$C2/c$
R_5^+	$(a,0,-a)$	$Imma$
Space group $C2/m$ with lattice vectors $(0,-2,0)(2,0,0)(0,1,1)$, origin $(\frac{1}{2},\frac{1}{2},0)$		
Γ_1^+	(a)	$Pm\bar{3}m$
Γ_2^+	(a)	$Pm\bar{3}$
Γ_3^+	(a,b)	$Pmmm$
Γ_4^+	$(a,0,0)$	$P4/m$
Γ_5^+	$(0,a,0)$	$Cmmm$
R_4^+	$(a,0,b)$	$C2/m$
R_5^+	$(a,0,b)$	$C2/m$

rich and La-rich compositions. The postulated intrinsic instability would couple bilinearly with the Jahn-Teller distortion to stabilize *Imma* and $C2/m$ structures in Pr-rich crystals but could drive a transition to $C2/c$ or $C2/m$ structures by itself in La-rich crystals. At a composition of approximately 30% Pr the *Imma* stability field ceases to exist and it is suggested here that this might represent the composition at which the Jahn-Teller effect is diluted out. The mechanism of softening is then entirely associated with the intrinsic instability. The elastic softening observed in pure $LaAlO_3$ is very slight[11] and the T_c^* value obtained from fitting the softening trend of Pr_1 falls below the trend for other compositions (Fig. 6). It appears, therefore, that size effects are important also for the postulated soft mode in that it is only weakly developed at and below 1% substitution of La by Pr. Based on results for the plateau effect in $PrAlO_3$,[32] this limit corresponds to the composition at which strain fields around individual Pr atoms would start to overlap with each other in the $LaAlO_3$ structure.

C. Dissipation behavior

Variations in the inverse quality factor, Q^{-1}, presented in Fig. 7 show changes in the dissipative behavior of the samples caused by changes in microstructure through transitions. These too form a consistent pattern across the solid solution. At high temperatures in the $R\bar{3}c$ stability field increased Q^{-1} for all samples follows the same trend as seen in $LaAlO_3$,[12] and is probably due to anelastic contributions from the motion of twin walls which develop as a consequence of the cubic-rhombohedral phase transition. Loss of resonance peaks (superattenuation) appears to be essentially the same at all compositions, implying that the La/Pr ratio does not influence the twin wall dynamics. At low temperatures Q^{-1} increases in the *Imma* stability field. The disappearance of peaks at the *Imma*-$C2/m$ transition for compositions Pr_{40}-Pr_{100} shows that the monoclinic phase gives rise to superattenuation in the same manner as at the $Pm\bar{3}m$-$R\bar{3}c$ transition in $LaAlO_3$ and the $Pm\bar{3}m$-$I4/mcm$ transition in $(Ca,Sr)TiO_3$[34] and pure $SrTiO_3$.[35] This implies that twin walls arising at the orthorhombic-monoclinic phase transition are highly mobile.

As already discussed by Carpenter *et al.*[8] there is a small temperature interval at approximately 90–116 K within the monoclinic phase of $PrAlO_3$ where peaks reappear. This is close to coinciding with a sharp minimum in a shear elastic constant detected by Brillouin scattering at 118 K (Ref. 36) and appears to be related directly to the development of a metrically tetragonal (monoclinic structure with tetragonal unit cell dimensions) structure at ~114 K. The metrically tetragonal structure would still contain monoclinic twin walls, but with no strain contrast across them, and hence would not contribute to any elastic softening if they were to move under an applied stress. This anomaly is not seen in any other samples, consistent with lattice parameter data of Carpenter *et al.*[3] which show that the metrically tetragonal configuration is not reached at other compositions.

Recently it has been shown that $PrAlO_3$ exhibits some anomalous magnetism in the $C2/m$ stability field.[37] This was explained by the existence of tetragonally distorted domains whose fourfold axis could be reoriented by the application of a magnetic field. Magnetic domain reorientation occurs via motion of twin walls and the evidence given here confirms that twin wall motion can occur easily in the $C2/m$ stability field. The same possibilities for controlling ferroelastic twin domains by a magnetic field as occurs in pure $PrAlO_3$ presumably exist across the solid solution at low temperature.

V. CONCLUSION

Pseudoproper ferroelastic softening across the entire $(La,Pr)AlO_3$ solid solution is consistent with the existence of an intrinsic zone-center instability in the structure, as suggested previously for pure $LaAlO_3$ by Carpenter *et al.*[11] It is unlikely that the weak Jahn-Teller effect for Pr^{3+} in 12-fold coordination could be responsible for this and the additional effect of a soft mode has been postulated. This develops more strongly as relatively large La^{3+} ions are replaced by smaller Pr^{3+}. One implication of such an elastic instability is that doping of $LaAlO_3$ with Pr might extend the variety of properties which can be induced in thin-film applications. Strong acoustic attenuation above 600 K in the stability field of the $R\bar{3}c$ structure is consistent with superattenuation by ferroelastic twin walls observed in other perovskites with octahedral tilting. The observation of superattenuation at low

temperatures in $(La,Pr)AlO_3$ crystals indicates that similar anelastic phenomena can occur in a monoclinic perovskite. Although $PrAlO_3$ is only paramagnetic, alignment of magnetized domains can be achieved by application of a magnetic field in the stability field of the monoclinic structure.[37] This appears to be facilitated by the mobility of monoclinic twin walls, offering a possibility of ferroelastic switching controlled by application of a magnetic field.

ACKNOWLEDGMENTS

S.T., D.A.P., and T.L. thank the FP7 NMP ENSEMBLE Project (Grant No. GA NMP4-SL-2008-213669) and the Ministry of Science and Higher Education of Poland (Grant No. N 5076 143 32/4056) for partially supporting this work. The RUS facilities in Cambridge were established through a grant from the Natural Environment Research Council of Great Britain (NE/B505738/1) to M.A.C.

[1] R. E. A. McKnight, B. J. Kennedy, Q. Zhou, and M. A. Carpenter, J. Phys.: Condens. Matter **21**, 015902 (2009).

[2] M. A. Carpenter and C. J. Howard, Acta Crystallogr., Sect. B: Struct. Sci. **65**, 147 (2009).

[3] M. A. Carpenter, C. J. Howard, B. J. Kennedy, and K. S. Knight, Phys. Rev. B **72**, 024118 (2005).

[4] V. K. Wadhawan, Phase Transitions **3**, 3 (1982).

[5] M. A. Carpenter and E. K. H. Salje, Eur. J. Mineral. **10**, 693 (1998).

[6] S. M. Moussa, B. J. Kennedy, B. A. Hunter, C. J. Howard, and T. Vogt, J. Phys.: Condens. Matter **13**, L203 (2001).

[7] R. J. Birgeneau, J. K. Kjems, G. Shirane, and L. G. Vanuiter, Phys. Rev. B **10**, 2512 (1974).

[8] M. A. Carpenter, E. C. Wiltshire, C. J. Howard, R. I. Thomson, S. Turczynski, D. A. Pawlak, and T. Lukasiewicz, Phase Transitions **83**, 703 (2010).

[9] T. J. Glynn, R. T. Harley, W. Hayes, A. J. Rushworth, and S. H. Smith, J. Phys. C **8**, L126 (1975).

[10] B. J. Kennedy, C. J. Howard, A. K. Prodjosantoso, and B. C. Chakoumakos, International Conference on Neutron Scattering, Munich, Germany, 09–13 September, 2001 [Appl. Phys. A: Mater. Sci. Process. **74**, S1660 (2002)].

[11] M. A. Carpenter, A. Buckley, P. A. Taylor, R. E. A. McKnight, and T. W. Darling, J. Phys.: Condens. Matter **22**, 035406 (2010).

[12] M. A. Carpenter, A. Buckley, P. A. Taylor, and T. W. Darling, J. Phys.: Condens. Matter **22**, 035405 (2010).

[13] R. W. Simon, C. E. Platt, A. E. Lee, G. S. Lee, K. P. Daly, M. S. Wire, and J. A. Luine, Appl. Phys. Lett. **53**, 2677 (1988).

[14] J. Zhu, Z. Liang, Y. R. Li, Y. Zhang, and X. H. Wei, J. Cryst. Growth **294**, 236 (2006).

[15] A. Masuno, T. Terashima, Y. Shimakawa, and M. Takano, Appl. Phys. Lett. **85**, 6194 (2004).

[16] A. Masuno, M. Haruta, M. Azuma, H. Kurata, S. Isoda, M. Takano, and Y. Shimakawa, Appl. Phys. Lett. **89**, 211913 (2006).

[17] A. Ohtomo and H. Y. Hwang, Nature (London) **427**, 423 (2004).

[18] U. Schwingenschlögl and C. Schuster, Chem. Phys. Lett. **467**, 354 (2009).

[19] M. Huijben, A. Brinkman, G. Koster, G. Rijnders, H. Hilgenkamp, and D. H. A. Blank, Adv. Mater. **21**, 1665 (2009).

[20] B. Lüthi and W. Rehwald, in *Structural Phase Transitions*, edited by K. A. Muller and H. Thomas, Topics in Current Physics (Springer-Verlag), Berlin, 1981, Vol. 23, p. 131.

[21] M. Born and K. Huang, *Dynamical Theory of Crystal Lattices* (Clarendon Press, Oxford, 1954).

[22] J. Czochralski, Z. Phys. Chem., Stoechiom. Verwandtschaftsl. **92**, 219 (1918).

[23] D. A. Pawlak, T. Lukasiewicz, M. A. Carpenter, M. Malinowski, R. Diduszko, and J. Kisielewski, J. Cryst. Growth **282**, 260 (2005).

[24] R. E. A. McKnight, T. Moxon, A. Buckley, P. A. Taylor, T. W. Darling, and M. A. Carpenter, J. Phys.: Condens. Matter **20**, 075229 (2008).

[25] A. Migliori and J. D. Maynard, Rev. Sci. Instrum. **76**, 121301 (2005).

[26] R. E. A. McKnight, M. A. Carpenter, T. W. Darling, A. Buckley, and P. A. Taylor, Am. Mineral. **92**, 1665 (2007).

[27] R. E. A. McKnight, C. J. Howard, and M. A. Carpenter, J. Phys.: Condens. Matter **21**, 015901 (2009).

[28] A. Migliori and J. L. Sarrao, *Resonant Ultrasound Spectroscopy: Applications to Physics, Material Measurements and Nondestructive Evaluation* (Wiley, New York, 1997).

[29] Z. Zhang, J. Koppensteiner, W. Schranz, J. B. Betts, A. Migliori, and M. A. Carpenter, Phys. Rev. B **82**, 014113 (2010).

[30] S. Cotton, *Lanthanide and Actinide Chemistry* (Wiley, New York, 2006).

[31] M. A. Carpenter, R. E. A. McKnight, C. J. Howard, Q. Zhou, B. J. Kennedy, and K. S. Knight, Phys. Rev. B **80**, 214101 (2009).

[32] M. Atanasov, C. Daul, H. U. Gudel, T. A. Wesolowski, and M. Zbiri, Inorg. Chem. **44**, 2954 (2005).

[33] V. S. Mironov and L. E. Li, J. Alloys Compd. **279**, 83 (1998).

[34] J. W. Walsh, P. A. Taylor, A. Buckley, T. W. Darling, J. Schreuer, and M. A. Carpenter, Phys. Earth Planet. Inter. **167**, 110 (2008).

[35] A. Migliori, J. L. Sarrao, W. M. Visscher, T. M. Bell, M. Lei, Z. Fisk, and R. G. Leisure, Physica B **183**, 1 (1993).

[36] P. A. Fleury, P. D. Lazay, and L. G. Vanuiter, Phys. Rev. Lett. **33**, 492 (1974).

[37] M. Wencka, S. Vrtnik, M. Jagodic, Z. Jaglicic, S. Turczynski, D. A. Pawlak, and J. Dolinsek, Phys. Rev. B **80**, 224410 (2009).